











Sentinel-1 Backscatter and Interferometric Coherence for Soil Moisture Retrieval in Winter Wheat Fields Within a Semiarid South-Mediterranean Climate: Machine Learning Versus Semiempirical Models

Jamal Ezzahar , Abdelghani Chehbouni , Nadia Ouaadi , Mohammed Madiafi , Khabba Said , Salah Er-Raki , *Member, IEEE*, Ahmed Laamrani , Adnane Chakir , Zohra Lili Chabaane , and Mehrez Zribi , *Senior Member, IEEE*

Abstract—This work aims to assess the effectiveness of machine learning (ML) algorithms and semiempirical models for surface soil moisture (SSM) retrieval by exploring the Sentinel-1 backscatter and interferometric coherence data. First, three commonly used categories of ML algorithms are evaluated using data gathered

from diverse rainfed and irrigated wheat fields located in Morocco and Tunisia. Specifically, these algorithms include artificial neural network (ANN), deep neural network, three support vector regression (SVR) models [radial basis function (SVR_rbf), linear (SVR_linear), and polynomial (SVR_quad) kernels], and two tree-based methods [random forest and eXtreme Gradient Boosting (XGBoost)]. The comparison between predicted and measured SSM showed that the best retrieval results were obtained using Sentinel-1 data at VV polarization with R ranging between 0.68 and 0.76 and root-mean-square error (RMSE) of $0.05 \text{ m}^3/\text{m}^3$ and $0.06 \text{ m}^3/\text{m}^3$. Second, to further assess their transferability, the ANN, SVR_rbf, and XGBoost, which demonstrated the most favorable results from each category, were evaluated and compared against the coupled Water Cloud and Oh models (WCM), using a second dataset collected over a drip-irrigated wheat field in Morocco. Overall, the best retrieval results were achieved by ANN and SVR_rbf with R and RMSE of 0.81 and $0.034 \text{ m}^3/\text{m}^3$, respectively. In addition, their performances were consistent with that of WCM, which yielded R and RMSE values of 0.81 and $0.04 \text{ m}^3/\text{m}^3$, respectively. Finally, due to its good compromise between retrieval accuracy of SSM, processing time, and simplicity, SVR_rbf was chosen to generate high-resolution SSM maps from Sentinel-1 data over irrigated wheat fields.

Manuscript received 5 May 2023; revised 19 September 2023 and 10 November 2023; accepted 27 November 2023. Date of publication 5 December 2023; date of current version 3 January 2024. This work was supported in part by the Project IRRIWELL (a novel plant-based approach to estimate irrigation water needs and the application of optimal deficit strategy, under Grant 01DH21016, 2021–2024), in part by the Project Rise-H2020-ACCWA under Grant 823965, in part by the Project PRIMA-S2-ALTOS-2018 “Managing water resources within Mediterranean agrosystems by accounting for spatial structures and connectivities,” in part by the Project ASSIWAT, in part by the Project IDEWA, and in part by the Project GEANTech. (Corresponding author: Jamal Ezzahar.)

Jamal Ezzahar is with the MISCOM, National School of Applied Sciences, Cadi Ayyad University, Marrakech 40000, Morocco, and also with the Center for Remote Sensing Application, Mohammed VI Polytechnic University, Ben Guerir 43150, Morocco (e-mail: j.ezzahar@uca.ma).

Abdelghani Chehbouni is with the Center for Remote Sensing Application, Mohammed VI Polytechnic University, Ben Guerir 43150, Morocco, and also with the CESBIO, IRD, Marseille, France (e-mail: abdelghani.chehbouni@um6p.ma).

Nadia Ouaadi is with the CESBIO, 31400 Toulouse, France (e-mail: nadia.ouaadi@gmail.com).

Mohammed Madiafi is with the MISCOM, National School of Applied Sciences, Cadi Ayyad University, Marrakech 40000, Morocco (e-mail: m.madiafi@uca.ac.ma).

Khabba Said is with the LMFE, Department of Physics, Faculty of Sciences Semlalia, Cadi Ayyad University, Marrakech 40000, Morocco, and also with the Center for Remote Sensing Application, Mohammed VI Polytechnic University, Ben Guerir 43150, Morocco (e-mail: khabba@uca.ac.ma).

Salah Er-Raki is with the ProcEDE, Department of Applied Physics, Faculty of Sciences and Technologies, Cadi Ayyad University, Marrakech 40000, Morocco, and also with the Center for Remote Sensing Application, Mohammed VI Polytechnic University, Ben Guerir 43150, Morocco (e-mail: s.erraki@uca.ma).

Ahmed Laamrani is with the Center for Remote Sensing Application, Mohammed VI Polytechnic University, Ben Guerir 43150, Morocco (e-mail: ahmed.laamrani@um6p.ma).

Adnane Chakir is with the LMFE, Department of Physics, Faculty of Sciences Semlalia, Cadi Ayyad University, Marrakech 40000, Morocco (e-mail: adnane.chakir@ird.fr).

Zohra Lili Chabaane is with the University of Carthage, National Agronomic Institute of Tunisia, LR17AGR01 InteGRatEd management of Natural resources: remote sensing, spatial Analysis and Modeling (LR GREEN-TEAM), Tunis 1082, Tunisia (e-mail: Zohra.LiliChabaane@inat.u-carthage.tn).

Mehrez Zribi is with the CESBIO, CNES/CNRS/INRAE/IRD/UT3-Paul Sabatier, Toulouse 31400, France (e-mail: Mehrez.Zribi@ird.fr).

Digital Object Identifier 10.1109/JSTARS.2023.3339616

Index Terms—Backscattering models, irrigated and rainfed winter wheat, machine learning (ML), semiarid regions, Sentinel-1 backscatter and interferometric coherence, surface soil moisture (SSM).

I. INTRODUCTION

IT IS well known that accurate estimates of surface soil moisture (SSM) are crucially required for a better understanding of water and energy exchanges at the biosphere–atmosphere interface [1] and hydrological processes [2], [3]. Indeed, SSM governs the energy balance equation at the land surface by influencing the partitioning of available energy into sensible and latent heat flux through soil evaporation and plant transpiration processes [4]. Thus, SSM controls the water budget equation through its impact on the partitioning of precipitation into runoff and infiltration [3]. In addition, the improvement of land surface models (LSMs) and distributed hydrologic models can benefit from realistic SSM values either as an initial condition or through assimilation techniques [5], [6], [7], [8], [9]. Meanwhile, SSM

has been recognized as an indispensable variable in climate studies by the Global Climate Observing System [10] due to its ability to provide valuable climate background by analyzing the long-term trends of its variations [3]. More specifically, precise SSM information is a key parameter for agricultural water resources management such as irrigation scheduling, hydric stress monitoring, and yield prediction, which can ensure food and water security, particularly in arid and semiarid regions [11], [12]. Consequently, an accurate knowledge of SSM at high spatiotemporal resolution exhibits an important source of information to both human activities and ecological environment.

Remote-sensing-based approaches that incorporate active microwave sensors (viz., synthetic aperture radar—SAR and scatterometers [13]) and passive microwave sensors (radiometers: e.g., AMSR-E [14], SMOS [15], and SMAP [16]) have been found to be promising due to their high sensitivity to SSM variations [17] and weather-independent capability compared to optical sensors [18]. These sensors are characterized by a coarse spatial resolution, of the order of tens of kilometers, which is a major drawback. Such a resolution is useful for climate applications, e.g., [19]. However, the estimation of variables that present a high spatial variability from one plot of less than one-tenth of a square kilometer to another requires finer resolution, such as that maintained by today's SAR sensors. In particular, the ESA Sentinel-1 constellation with two satellites A and B, launched in 2014 and 2016, respectively, has opened up new research opportunities for retrieving SSM at the field scale, thanks to their high spatial resolution (10 m) and revisit times of up to 6 days [20]. In a recent study in [21], attention was drawn to the collaborative utilization of SMAP and Sentinel-1 backscatter data. This approach aims to extend the downscaling of SMAP soil moisture beyond the 1-km scale, necessitating further modifications to address the existing challenges related to achieving subkilometer spatial resolutions. These adjustments are specially tailored to suit the requirements of the Southern Mediterranean region.

The retrieval of SSM from SAR data is, nonetheless, not a straightforward task due to the nonlinear dependence between radar signal and in situ SSM [19]. To address this issue, numerous physically-based scattering models have been developed such as Michigan microwave canopy scattering (MIMICS, [22]) and Karam [23]. As a result of their strong physical foundation, these models are more suited for characterizing the vegetation layer in depth and accurately modeling backscattering from vegetated surfaces [24]. However, these models are difficult to implement through SSM inverting algorithms, particularly at a large scale, due to their necessity of several input parameters mainly including information about soil surface characteristics, leaves, branches, trunks, and sensors. In addition, the use of these models requires substantial knowledge of the complex mechanisms involved in the interaction of electromagnetic radiation and the target variable. Likewise, the coupling of semiempirical models, such as the Oh model [25] for bare soil and the Water Cloud model [26] for vegetation, has been widely used, particularly for crops such as wheat. This is due mainly to their good tradeoff between accuracy and model complexity [27], [28], [29], [30], [31], [32], [33], [34]. Nevertheless, the applicability of

this category of models to other conditions and vegetation types is still an open question due to their dependence on observation data related to vegetation and soil surface roughness [36]. In fact, even with extensive in situ sampling of surface roughness, it is still challenging to provide an accurate roughness parameterization scheme at the field scale or larger because of the natural variability of the soil [35], [36], [37].

These difficulties associated with physical and semiempirical approaches have forced researchers to look for purely data-driven predicting tools by exploring the recent development of machine learning (ML) algorithms [1], [38], [39]. As a matter of fact, ML algorithms, which are based on statistical learning theory, are able to learn independently the high nonlinear relationship between SSM (target) and land surface features (predictors) at the global scale. More recently, the utilization of ML algorithms has gained increased attention in SSM retrieval due to their ability to tackle numerous limitations of the semiempirical and physically based models as previously outlined. Most of the previous studies focused on the joint use of radar data and optical data (as a descriptor of vegetation) as input features for training their ML algorithms and thus retrieving SSM [19], [40], [41], [42], [43]. However, a severe lack of optical data observations may occur in the event of prolonged cloud cover, which is quite frequent when crops, particularly cereals, are cultivated during the wet season, as in the South-Mediterranean regions. To deal with this issue, Efremova et al. [44] have proposed a framework for unsupervised deep domain adaptation for radar and optical satellite imagery with cycle-consistent adversarial networks (cycleGANs). In the same vein, using a large in situ database collected from several irrigated and rainfed wheat in Morocco and Tunisia countries, Ouaadi et al. [45] have developed a new approach to predict SSM, based only on two complementary and relatively independent information extracted from Sentinel-1 radar including backscattering coefficient and interferometric coherence (ρ). According to their finding, ρ , which is defined as the variance of the interferometric phase, can be fairly used as a descriptor of vegetation thanks to its good correlation with vegetation characteristics such as the dry above-ground biomass and the vegetation water content. In addition, they showed that the use of ρ as a descriptor improves the SSM retrieval compared to the Normalized Difference Vegetation Index (NDVI) derived from Sentinel-2. Lately, Villarroya-Carpio et al. [46] have successfully demonstrated the Sentinel-1 coherence's usefulness as a vegetation index by relying on its high correlation with NDVI revealed over several crops. Likewise, they pointed out that both its temporal evolution and the main phenological stages of crops are well matched. Note that these recent works confirm the findings reported previously in several studies, which have already been exhibited that ρ is tightly related to vegetation characteristics [47], [48], [49]. Overall, these findings support the use of solely radar data in the SSM inversion process, excluding optical data that are limited by weather and lighting conditions.

The objective of this study is to evaluate the utilization of radar data, specifically Sentinel-1's backscattering coefficient and coherence, through the implementation of multiple ML algorithms, for SSM monitoring. Indeed, as far as we know, no investigation

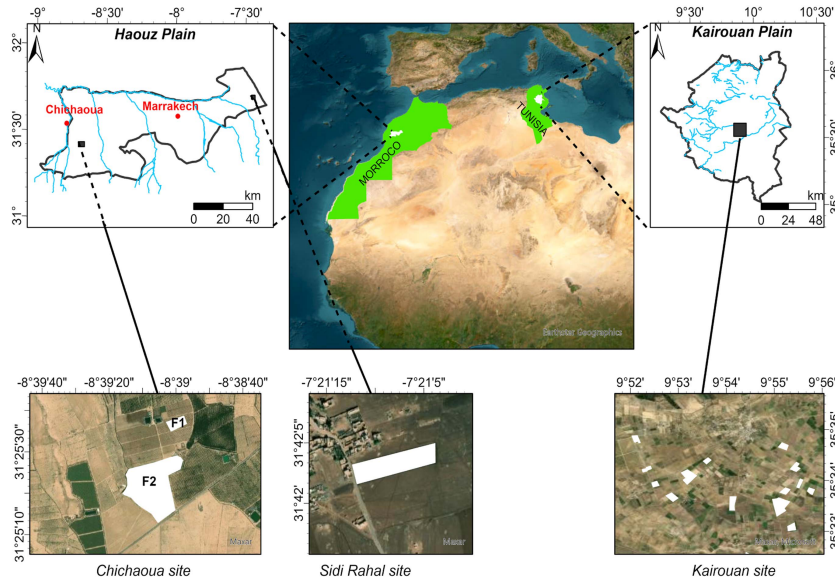


Fig. 1. Location of Sidi Rahal and Chichaoua sites in the Haouz plain, central of Morocco as well as the Kairouan sites in the Kairouan plain.

TABLE I
GENERAL INFORMATION ABOUT THE SSM MEASUREMENTS OVER THE DIFFERENT WINTER WHEAT SITES IN MOROCCO AND TUNISIA

Site	Number of plots	Season	Irrigation system	SSM measurements	Calculated of SSM	Range of SSM (m^3/m^3)
Kairouan	6	November 2016–April 2017	Rainfed	Handheld theta probe (20 samples in each field)	Average of 20 samples	0.05–0.5
	12		Sprinkler			
Sidi Rahal	1	November 2016–June 2017 and November 2017–June 2018	Rainfed	2 TDR sensors at 5 cm	Average of 2 TDR measurements	0.04–0.39
Chichaoua	2 (F1 and F2)	November 2016–June 2018 (F1) and November 2018–June 2019 (F2)	Drip	2 TDR sensors at 5 cm	Average of 2 TDR measurements	0.06–0.34

has highlighted the drive of ML algorithms directly by coherence as a descriptor of vegetation and backscattering coefficient. This study will focus on testing the most popular ML regression algorithms such as artificial neural network (ANN) and deep neural network (DNN), support vector regression (SVR) [viz., radial basis function (SVR_rbf), polynomial (SVR_quad), and linear (SVR_linear)] and tree-based [viz., random forest (RF) and eXtreme Gradient Boosting (XGBoost)]. This work will also assess the transferability of these algorithms as well as their performance against the coupled Water Cloud and Oh models (WCM). To this end, data were collected over irrigated and rainfed winter wheat fields in Morocco and Tunisia within the framework of the Tensift and Kairouan network observatories.

II. DATA DESCRIPTION AND METHODOLOGY

A. Experimental Data

In order to test the potential of the ML algorithms and their transferability to retrieve SSM, several rainfed and irrigated wheat sites located in the Haouz plain (center of Morocco) and Kairouan plain (center of Tunisia) were used in this

study (see Fig. 1). Both sites are characterized by a semi-arid Mediterranean climate with high potential evaporation (about 1600 mm per year), greatly exceeding the annual rainfall, which ranged between 250 and 300 mm. Descriptive details of both sites are detailed in [31] and [45]. SSM measurements were conducted using a time-domain reflectometer (TDR Campbell Scientific CS616) and handheld theta probe sensors at different wheat fields in Haouz and Kairouan sites, respectively. In addition, these measurements were properly calibrated using the gravimetric method. Data used in this study were recorded from three sites (see Table I).

- 1) *Kairouan site*: In total, 18 fields of irrigated (sprinkler technique) and rainfed wheat located in the Kairouan plain were selected [31]. Twenty handheld theta probe samples were recorded from different locations in each field and were averaged per field. These measurements were performed at topsoil (i.e., a depth of 5 cm) and taken at the same time as Sentinel-1 acquisitions over the chosen fields.
- 2) *Sidi Rahal site*: One rainfed wheat field situated approximately 40 km east of Marrakech city (Haouz plain) was selected [50]. Automated SSM measurements were

obtained through the use of two TDR sensors positioned at a depth of 5 cm and subsequently averaged.

- 3) *Chichaoua site*: Two irrigated wheat fields (referred to hereafter as F1 and F2) within a private farm were selected. This farm is situated near the province of Chichaoua at 65 km west of Marrakesh city (Haouz plain). Data were recorded in these fields during three growing seasons. The first field was monitored during the two growing seasons 2016–2017 and 2017–2018 while the second one was monitored during the 2018–2019 growing season. In both fields, drip irrigation was applied, with a flow rate of 7.14 mm/h for each dripper. Automated SSM measurements were collected using two TDR sensors positioned between and beneath the drippers at a depth of 5 cm. These measurements were then averaged to offer a more representative value for the Sentinel-1 pixel.

Note that in this work, SSM data collected over Kairouan and Sidi Rahal fields were used for the training and validation process of the ML algorithms while that collected over Chichaoua site (i.e., F1 and F2) were explored to test their transferability and to evaluate their performances against the coupled WCM model built through the combination of backscattering of soil (Oh) and vegetation (Water Cloud) models. In addition, measurements of the field’s surface roughness were taken using a pin profiler of 1-m length with 2 cm between two successive needles in order to run the WCM model. Sixteen samples were gathered at various locations over the experimental field, with eight measurements parallel to the row and eight perpendicular to the row to better account for the influence of row direction. Thanks to an algorithm based on needle height normalization, these measurements were processed to provide two statistical roughness parameters used as inputs of the Oh model such as the root-mean-square surface height (h_{rms}) and the correlation length [45]. Likewise, 11 hemispherical digital images were taken weekly at different locations over the experimental field to calculate the canopy fraction cover used as an input of the Water Cloud model.

B. Satellite Data

This study used the Sentinel-1 radar data for retrieving SSM including the backscattering coefficient and the coherence at VV and VH polarizations. Sentinel-1 consists of two identical satellites, Sentinel-1A and Sentinel-1B. Sentinel-1A was launched on April 3, 2014, whereas Sentinel-1B was launched on April 25, 2016. Both satellites are equipped with a C-band SAR system in three different imaging modes, providing all-weather and day-and-night imaging capability with a revisit time of six days [20]. The interferometric wide-swath mode is the main operational imaging mode over land surfaces, realizing acquisitions in VV and VH polarizations over a wide-area coverage with a swath of up to 250 km and a resolution of up to 5×20 m. Note that, level-1 products, which can be directly downloaded from the Sentinel-1 mission’s official data hub, are typically distributed in the single look complex (SLC) and ground range detected (GRD) formats. Herein, a brief description of the GRD and SLC image processing is given, more details are given in [51]. GDR images

were processed at the original 10 m resolution with the Orfeo ToolBox (OTB) software [52] in order to compute the backscattering coefficient σ^0 . The main processing steps included in this software are: 1) thermal noise removal, 2) radiometric calibration [53], and 3) terrain correction [54] using digital elevation model (DEM) Shuttle Radar Topography Mission (SRTM) at 30-m resolution [55]. Also, SLC images were processed using the Sentinel application platform SNAP to derive the coherence, which typically ranges between 0 (incoherence) and 1 (perfect coherence). This process includes the following five steps.

- 1) The “Apply-Orbit-file” module to more accurately estimate the satellite’s location and speed.
- 2) The orbital data and the DEM SRTM were used to co-register (“Back-geocode”) the two consecutive images.
- 3) The application of the coherence module.
- 4) The TOPSAR-Deburst module was applied to remove the bursts (the black band in the SLC products).
- 5) Terrain correction was utilized to project the images on the Earth’s surface using the SRTM DEM.

Table II summarizes the characteristics of Sentinel-1 processed products across all fields used in the context of this study.

C. Methodology

Fig. 2 graphically summarizes the methodology and the various tasks performed in this study. In general, this research was structured into two main phases, involving the exploration of processed Sentinel-1 backscatter and interferometric coherence data in both VV and VH polarizations, along with ground data collected from various rainfed and irrigated wheat fields at three different sites, namely Kairouan, Sidi Rahal, and Chichaoua. In the first phase, an effort was made to assess the potential of three commonly used categories of ML algorithms to determine the best model within each category for the exclusive purpose of retrieving SSM based solely on Sentinel-1 data. These three categories, which are thoroughly explained in the Appendix, consist of algorithms utilizing neural networks (comprising ANN and DNN), support vector machines with radial basis function (SVR_rbf), linear (SVR_linear), and polynomial (SVR_quad) kernels, and tree-based algorithms (RF and XGBoost). All of these algorithms were trained and validated using data collected from a variety of rainfed and irrigated wheat fields situated in the Sidi Rahal and Kairouan sites. Following a comparison between the retrieved and measured SSM, a model was selected from each category based on its statistical performance metrics [root-mean-square error (RMSE), R^2 , and BIAS].

In the second phase, the selected models were examined for their transferability to improve their usability across diverse conditions, employing different datasets gathered from drip wheat fields situated in the Chichaoua site. Simultaneously, these models were assessed in comparison to the Water Cloud Model (WCM), which employs the same inputs, including backscatter coefficient and coherence, along with additional parameters, such as fractional cover and roughness. The outcomes generated by the selected ML models and the WCM were compared against the observed values to determine which model was most suitable

TABLE II
CHARACTERISTICS OF SENTINEL-1 PROCESSED PRODUCTS ACROSS ALL FIELDS USED IN THE CONTEXT OF THIS STUDY

Site	Season	Relative orbit number	Incidence angle	Relative orbit	Overpass time	Product	Number of images
Chichaoua (F1)	October 2016–July 2018	52	35.2°	descending	06:30	GRD SLC	110 106
Chichaoua (F2)	November 2018–May 2019	52	35.2°	descending	06:30	GRD SLC	31 30
Sidi Rahal	November 2016–June 2018	154	40°	descending	06:28	GRD SLC	61 60
Kairouan	November 2016–April 2017	88 and 95	39.5°–40°	Ascending and descending	17:20 and 05:21	GRD SLC	14 14

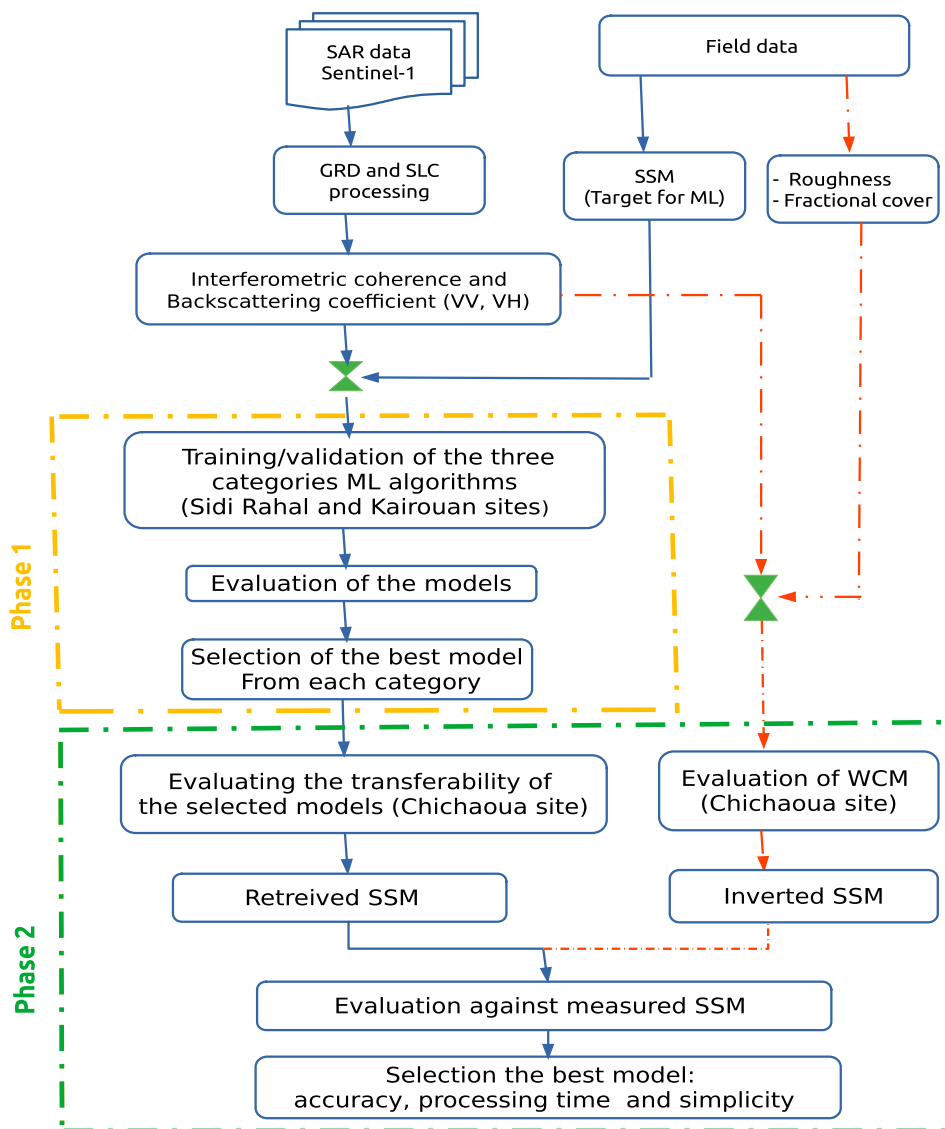


Fig. 2. Flowchart providing an overview of the methodology used in this work.

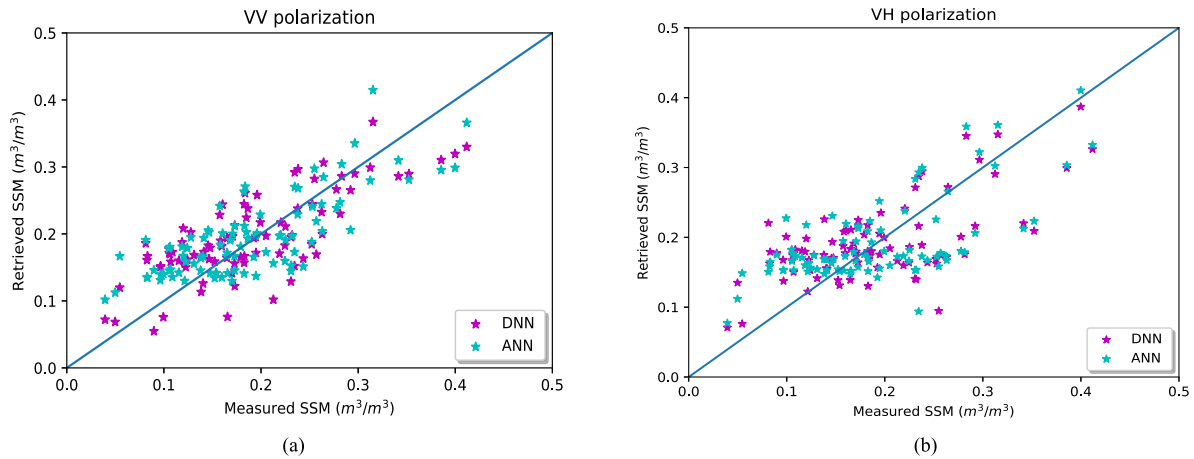


Fig. 3. Retrieved SSM using ANN and DNN algorithms versus in situ measurements over the Sidi Rahal and Kairouan sites. (a) VV polarization. (b) VH polarization.

for SSM mapping. This assessment is based on three criteria: 1) accuracy, 2) computational time, and 3) simplicity.

III. RESULTS AND DISCUSSION

In this study, the collected data over Morocco and Tunisia rainfed and irrigated winter wheat sites were combined and used to train and validate all ML methods. To this end, the data were subdivided into a training (calibration dataset) and a validation set. The backscatter coefficient and interferometric coherence at both polarization VV and VH were used as input and the measured soil moisture (MSM) as a target. Using multiple data sites has allowed us to build robust ML algorithms able to generate the simulated SSM from Sentinel-1 data over different regions. Subsequently, to enhance their applicability across various conditions, the most successful algorithms from the three categories were further tested on winter wheat sites with drip irrigation in Morocco. These algorithms were then compared to conventional techniques based on the inversion of vegetation and soil semiempirical models. This section is divided into three parts. The first part involves evaluating algorithms from three categories and selecting the best model from each category. The subsequent part focuses on investigating the transferability of the selected algorithms and conducting a comparison of these algorithms with WCM. Finally, the third part is dedicated to generating SSM maps using the algorithm that exhibits the best performance.

A. Evaluation of ML Algorithms

1) *ANN Versus DNN*: This section addresses the investigation of retrieving SSM using ANN and DNN algorithms based on the backscattering coefficient and interferometric coherence data for both VV and VH polarizations. In Fig. 3, a scatter plot depicting the relationship between retrieved and measured SSM is presented. Overall, both algorithms yielded quite good results between retrieved and measured SSM for VV polarization as shown in Fig. 3(a). The R , RMSE, and Bias values for DNN simulations were approximately 0.75, $0.05 \text{ m}^3/\text{m}^3$, and

$0.01 \text{ m}^3/\text{m}^3$, whereas for ANN, they were 0.76, $0.05 \text{ m}^3/\text{m}^3$, and $0.01 \text{ m}^3/\text{m}^3$, respectively (see Table III). It can be clearly observed that the obtained results are very similar, demonstrating the potential of ANN and DNN algorithms for retrieving SSM using only the Sentinel-1 backscatter and interferometric coherence as a vegetation descriptor at VV polarization. It should be noted that the use of interferometric coherence as a description of vegetation in conjunction with the backscatter coefficient as input for the ANN algorithm yielded approximately the same correlation between retrieval and MSM cited in [19]. Contrary to our investigation, Santi et al. [19] have trained their ANN algorithm using backscatter coefficient data generated through the implementation of a semiempirical model while the validation was conducted using data obtained directly from C-band and X-band at VV polarization, with NDVI employed as an optical descriptor for vegetation. Their finding showed that the RMSE and Bias values were $0.052 \text{ m}^3/\text{m}^3$ and $0.009 \text{ m}^3/\text{m}^3$ for C-band and $0.052 \text{ m}^3/\text{m}^3$ and $0.003 \text{ m}^3/\text{m}^3$ for X-band. Likewise, they pointed out that the use only of backscatter coefficient data without ancillary information of vegetation yielded a worst correlation between RSM and MSM. El Hajj et al. [40] have also proven that ANN driven by the backscatter coefficient at VV polarization and NDVI derived from Sentinel-1 and -2 provide satisfactory simulations of soil moisture and were well compared to our findings. Furthermore, the positive outcomes of our algorithms provide additional support to recent research conducted by Ouaadi et al. [45], which highlighted the capacity of backscatter coefficients and interferometric coherence at VV polarization for soil moisture retrieval through the inversion of the combined Oh and Water Cloud model, utilizing the same dataset. Their obtained values of R , RMSE, and Bias ranged between 0.7–0.75, 0.06 – $0.08 \text{ m}^3/\text{m}^3$, and 0.01 – $0.03 \text{ m}^3/\text{m}^3$, respectively.

On the contrary, the use of the backscatter coefficient and the interferometric coherence at VH polarization showed more dispersion for both algorithms ANN and DNN compared to VV polarization, as shown in Fig. 3(b). The values of R , RMSE, and Bias were about 0.54, $0.07 \text{ m}^3/\text{m}^3$, and $0.00 \text{ m}^3/\text{m}^3$ for

TABLE III
 STATISTICAL METRICS OF THE RETRIEVED SSM USING THE SEVEN ML ALGORITHMS INCLUDING THE RMSE, THE MEAN DIFFERENCE (BIAS), THE CORRELATION COEFFICIENT (R), THE SLOPE AS WELL AS THE OFFSET OF THE LINEAR REGRESSION

	R		RMSE (m ³ /m ³)		Bias (m ³ /m ³)		slope		intercept (m ³ /m ³)	
	VV	VH	VV	VH	VV	VH	VV	VH	VV	VH
DNN	0.75	0.62	0.05	0.06	0.01	0.00	0.94	0.88	0.0	0.02
ANN	0.76	0.64	0.05	0.06	0.01	0.00	1.01	0.87	-0.01	0.02
SVR_rbf	0.76	0.62	0.05	0.06	0.00	0.00	0.97	0.83	0.01	0.03
SVR_quad	0.74	0.56	0.05	0.06	0.00	0.00	0.92	0.72	0.02	0.05
SVR_linear	0.68	0.57	0.06	0.06	-0.01	-0.01	0.96	0.92	0.01	0.02
XGBoost	0.74	0.57	0.05	0.06	0.00	0.00	0.96	0.8	0.01	0.04
RF	0.69	0.51	0.06	0.07	0.00	-0.01	0.76	0.66	0.04	0.07

DNN simulations and 0.64, 0.06 m³/m³, and 0.00 m³/m³ for ANN. Scientifically speaking, this result is expected due to the fact that radar backscattering at VV polarization is generally more sensitive to the change in soil water content compared to VH polarization [56], [57], and the coherence at VV is the best describing of the crops such cereals (particularly for the wheat as in our case) contrary to VH, which better suited for certain less dense crops as stated in [46]. In the same vein, by inverting the combined model of Oh and WCM, Ouadi et al. [45] point out that the use of radar data (i.e., backscatter coefficient and the interferometric coherence) at VH polarization yielded more dispersion compared to VV polarization. In the same context, El Hajj et al. [40] have shown that ANN driven by the backscatter coefficient at VV polarization and NDVI derived from Sentinel-1 and -2 performed better than the use of VH polarization. By the same token, by exploring Sentinel-1 and Landsat 8 data, Bao et al. [58] have also reported that the backscattering at VV is more appropriate for soil moisture retrieval with an improvement of about 10% and 21% in R and RMSE compared to VH polarization.

Overall, in our specific study, we have noticed that the performance of single-layer ANN mimics the highly complex multilayers DNN in terms of statistical results at VV polarization. May be this behavior can be related to the fact that multilayers DNN needs more data and is devoted to a more complex problem, particularly when the estimated target depends on several input variables. Interestingly, as demonstrated in [59], the predictive performance of multilayers DNN increases strongly with the use of a large dataset. In the same vein, as stated in [60], the use of single-layer ANN can be considered as the potential algorithm for providing satisfactory soil moisture simulations from soil suction rather than the use of highly complex multilayers DNN, peculiarly under wetting conditions where it overfits the soil moisture.

Wherefore, based on these results and considering the computational time associated with each algorithm, we have decided to use only the single-layer ANN in the upcoming comparison with other ML algorithms and for the transferability evaluation.

This choice is made because the multilayer DNN algorithm did not yield a significant improvement in the estimation of SSM, at least within the context of our specific site conditions.

2) *SVR and Tree-Based Algorithms*: In this section, SVR (SVR_rbf, SVR_quad, and SVR_linear) and tree-based (XGBoost and RF) algorithms were evaluated using the same data explored in the training and testing process for the single-layer ANN. Similarly to the single-layer ANN, these five algorithms were trained and tested using data at both polarization VV and VH in order to confirm our findings concerning the potential of VV polarization for retrieving SSM. Figs. 4 and 5 exhibit the comparison between measured and retrieved SSM using the five algorithms at both VV and VH polarizations, respectively.

Regarding the results of SVR algorithms, the RBF kernel outperformed slightly based on the polynomial kernel in predicting soil moisture at VV polarization (see Table III). Both SVR models yielded the same values of RMSE (i.e., 0.05 m³/m³) and Bias (i.e., 0.00 m³/m³) with a small difference in R of 2%. Also, the obtained slope of the regression equation for SVR_rbf was close to 1 (about 0.97) while SVR_quad showed an underestimation of 8%. Globally, their performances are in accordance with the ANN algorithm. However, the linear kernel model performed less well than SVR_rbf and SVR_quad with R , RMSE, and Bias values of about 0.69, 0.06 m³/m³, and -0.01 m³/m³, respectively. It is important to mention that our findings were similar to those reported in previous studies [60], [61], which demonstrated that the SVR_rbf provides the most superior simulation results, followed by polynomial kernel and linear kernel. In a similar vein, our statistical metrics are in the range of the performance exhibited by the investigation in [43] when using SVR with several features extracted from Sentinel-1 and -2 and Radarsat-2 remote sensing data. Likewise, Katagis et al. [62] showed that the SVR algorithm driven by backscatter at VV polarization extracted from the active microwave Advanced Scatterometer (ASCAT) estimates correctly soil moisture and their results, which are in agreement with our findings, exhibit minor variations depending on the different training/testing configurations. Kindly note that,

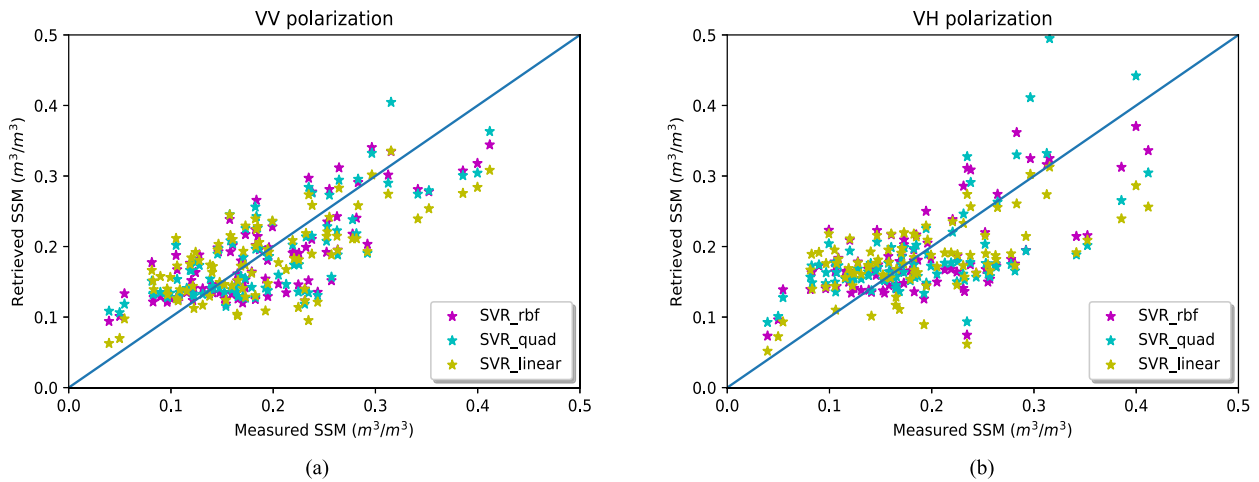


Fig. 4. Retrieved SSM using the support vector algorithms (RBF, quadratic, and linear kernels) versus in situ measurements over the Sidi Rahal and Kairouan sites. (a) VV polarization. (b) VH polarization.

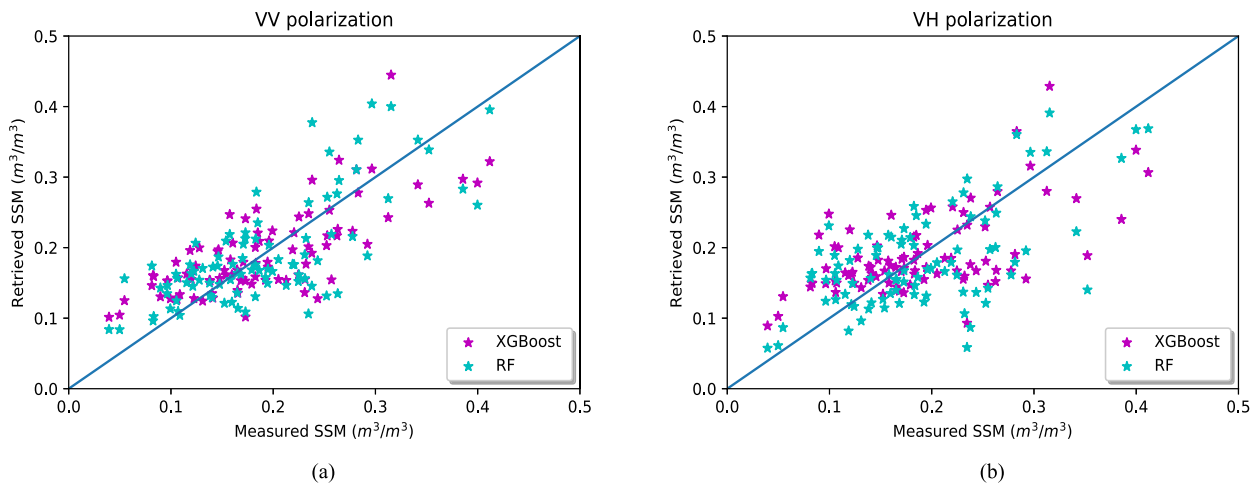


Fig. 5. Retrieved SSM using the XGBoost and RF algorithms versus in situ measurements over the Sidi Rahal and Kairouan sites. (a) VV polarization. (b) VH polarization.

in addition to its robustness in the estimation of soil moisture, and compared with SVR_quad, SVR_rbf exhibits lower computational complexity and less computational time [61]. Consequently, among the three proposed SVR algorithms, only the RBF kernel will be adopted for testing the transferability processes.

Concerning the tree-based algorithms, the comparison of retrieved soil moisture using XGBoost regression and RF regression (RFR) at VV polarization against the measured values is displayed in Fig. 5. According to Table III, XGBoost remarkably outperformed RF. While XGBoost achieved a satisfactory highest prediction accuracy with $R = 0.74$, $RMSE = 0.05 \text{ m}^3/\text{m}^3$, and an underestimation of 4%, RFR produced less prediction performance with $R = 0.69$, $RMSE = 0.06 \text{ m}^3/\text{m}^3$, and its values are shown to be noticeably underestimated compared to measured ones with about 24%. This good achievement of the XGBoost against RF is revealed also in [63] when they tested these algorithms by fusing several remote sensing data including data Sentinel-1 C-band dual polarimetric SAR, Sentinel-2

multispectral data, and ALOS Global Digital Surface Model to predict soil moisture in Australia. Compared to ANN and SVR algorithms, one can notice that the performance of XGBoost in the estimation of soil moisture is comparable to those obtained by SVR with RBF kernel and ANN algorithms. Moreover, RF yielded the worst performance among all the ML techniques regarding its underestimation in the retrieving of soil moisture. Subsequently, thanks to this evaluation between the two tree-based algorithms, only the XGBoost technique will be used concerning the investigation of the transferability processes.

Finally, as expected, the five algorithms including SVR with its three versions, XGBoost regression and RF produced the lowest prediction performance at VH polarization compared to VV polarization as shown in Figs. 4 and 5. According to Table III, slope and R are reduced by 0.2 and 0.18 for the polynomial kernel, 0.14 and 0.14 for the RBF kernel, 0.04 and 0.11 for the linear kernel, 0.16 and 0.17 for XGBoost, and 0.1 and 0.18 for RF. Furthermore, RMSE values were increased by about 10%, except for the linear kernel, which kept the same value.

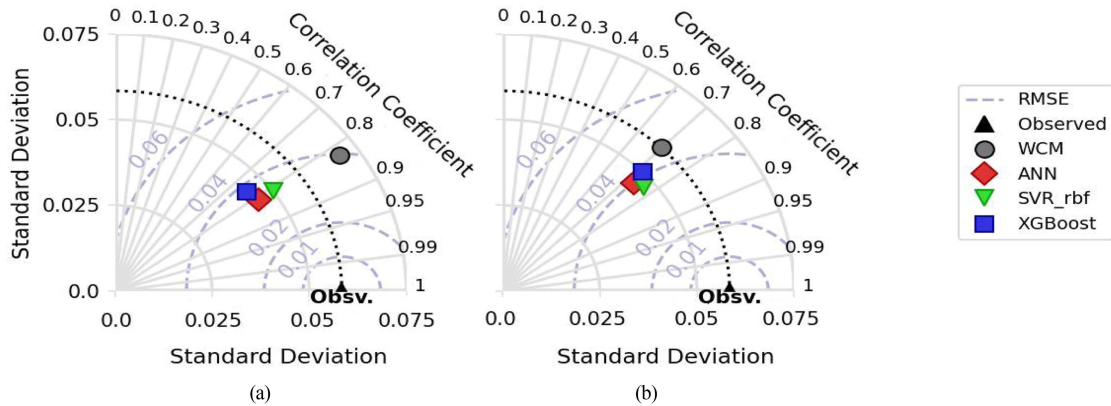


Fig. 6. Taylor diagrams for the ANN, SVR_rbf, XGBoost, and WCM for Chichaoua site. The solid line and dotted line represent the correlation coefficient and RMSD values.

TABLE IV
STATISTICAL METRICS OF THE RETRIEVED SSM USING SVR_RBF, ANN, XGBOOST, AND WCM AT VV AND VH POLARIZATION OVER CHICHAOUA SITE

	ANN		SVR_rbf		XGBoost		WCM	
	VV	VH	VV	VH	VV	VH	VV	VH
R	0.81	0.73	0.81	0.77	0.76	0.71	0.82	0.69
RMSE (m^3/m^3)	0.03	0.04	0.03	0.04	0.04	0.04	0.04	0.05
Bias (m^3/m^3)	0.002	0.004	-0.003	0.003	0.004	0.003	-0.004	0.05

Generally speaking, this finding confirms strictly the results obtained when we used the ANN algorithm and also the investigation in [45], which have stated that the use of the backscatter coefficient and the interferometric coherence at VV polarization can accurately estimate soil moisture through backscattering modeling inversion approach. In addition, all ML algorithms showed decreased performance for both polarizations when the SSM values exceeded $0.3 \text{ m}^3/\text{m}^3$. This phenomenon is linked to the saturation of the radar signal in regions with high soil moisture, which leads to a reduction in the accuracy of the inversion results.

B. Transferability of ML Algorithms and Their Evaluation Versus Backscattering Models

In order to test the transferability of the selected ML algorithms based on their highest prediction accuracy for the soil moisture estimation (ANN, SVR_rbf, and XGBoost), datasets collected over a drip-irrigated winter wheat field are employed. Over this area, Sentinel-1 data including the backscatter coefficient and the interferometric coherence are provided at 35.2° of the incidence angle. This will permit us to investigate also the effect of incidence angle on the SSM retrieval. Also, the performance of ML algorithms was evaluated against the coupled WCM. The performance of different ML algorithms as well as the WCM model to retrieve SSM at VV and VH polarization was investigated using a Taylor diagram (see Fig. 6). This presentation graphically summarizes the comparison between

ML algorithms and WCM model against the observations based on the root-mean-square difference (RMSD), the correlation coefficient R , and the standard deviations [64]. Statistical metrics are reported in Table IV.

As shown in Fig. 6 and Table IV, one can clearly see that at VV polarization both SVR_rbf and ANN algorithms achieved a high prediction accuracy and the performances are quite similar with R and RMSE values of about 0.81 and $0.03 \text{ m}^3/\text{m}^3$. Likewise, at VH polarization, both algorithms provided also quite similar performance but slightly lower than that obtained at VV polarization with RMSE of $0.04 \text{ m}^3/\text{m}^3$ and R of 0.73 (ANN) and 0.77 (SVR_rbf). Overall, these achieved satisfactory performances substantiate clearly the transferability of SVR_rbf and ANN algorithms, meaning the possibility of their use over other sites. Besides, compared to the statistical metrics at 40° of incidence angle obtained for the testing process, one can state that this finding confirms that the prediction performance increases significantly with lower angle incidence values. Indeed, as stated in [45], the Sentinel-1 signal is highly sensitive to soil moisture for low incidence angles and VV polarization. In the same vein, Zribi et al. [65] showed that the effect of vegetation and surface roughness is more stronger on the radar signal at 40° .

By contrast, the predictions of XGboost were lower than those for SVR_rbf and ANN algorithms at both polarizations. The obtained values of R at VV and VH were 0.76 and 0.71, respectively, while the RMSE was equal to $0.04 \text{ m}^3/\text{m}^3$ for

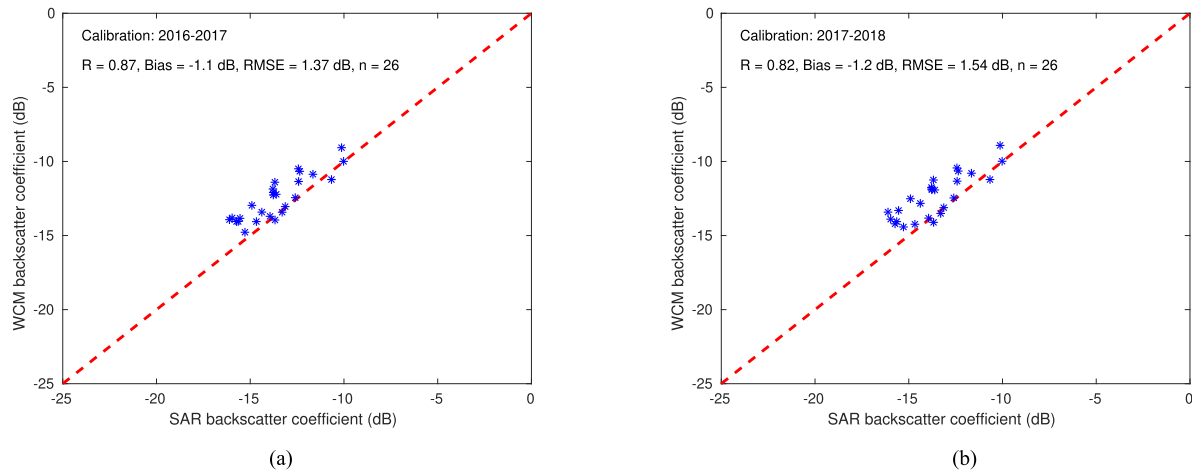


Fig. 7. Comparison between backscattering coefficients derived from Sentinel-1 images and those simulated by WCM at VV polarization over F2 using the calibrated values of A and B obtained over F1 during the (a) 2016–2017 and (b) 2017–2018 seasons.

both polarization. Therefore, it can be concluded that SVR_rbf and ANN are still the suitable algorithms for soil moisture retrieval at VV polarization, and thus, the discussion concerning the evaluation of ML against the coupled model WCM will be focused thereafter only on these two algorithms. Note that data collected from the first season (2016–2017) over F1 were used for calibration of WCM while that of the second season (2017–2018) and F2 data (season 2018–2019) were used for validation. So, as shown in Fig. 6, the metrics of WCM were slightly close to those procured by both algorithms. At VV, R and RMSE values were 0.82 and $0.04 \text{ m}^3/\text{m}^3$, respectively, and the values of these coefficients at VH were 0.69 and $0.05 \text{ m}^3/\text{m}^3$, respectively. However, in spite of its good achievement, WCM is still site-specific due to its strong dependence on two empirical factors A and B (10) and (11), meaning that its performance can drop drastically when growth conditions diverge significantly, in terms of canopy structure in particular, from the conditions on which the calibration is made. To illustrate this issue, an investigation is made to simulate the backscatter coefficient at VV over F2 using two couple optimized values of A and B obtained over F1 during the first and second seasons 2016–2017 and 2017–2018. Fig. 7 exhibits the comparison between backscattering coefficients derived from Sentinel-1 images and those simulated by WCM. The statistical metrics show clearly that the performance is improved when data of the 2016–2017 season are used with an increase in R of 0.05 and a decrease in RMSE of 0.13 dB. This can undoubtedly impact the soil moisture inversion using the Water Cloud Model (WCM), as elaborated in [45], where they assessed the retrieval of soil moisture over a different wheat field sown during the same time as F1. The data of the 2016–2017 season are used for calibration and that of 2017–2018 for validation. Their finding exhibited a poor performance of WCM even though the calibration was done over the same field due to differences between the two seasons, mainly related to the invasion of the adventices with strong horizontal development in the validation period. As far as we know, no previous studies have investigated the evaluation of coupling two radar backscattering models in order to take into

account soil and vegetation contributions and ML algorithms to assess soil moisture based only the radar data. To date, [50] have evaluated SVR against the theoretical integral equation model (IEM) to retrieve soil moisture over bare agricultural soil in the Tensfit basin of Morocco. They concluded that the SVR driven only by the backscatter coefficient can be a good algorithm for large-scale soil moisture monitoring instead of IEM that requires additional spatial measurements of root-mean-square height (h_{rms}), which is not an easy task, particularly over heterogeneous areas. Likewise, using dual-polarized Sentinel-1 backscattering coefficients and NDVI derived from Sentinel-2 collected over the south of Tunisia, Inoubli et al. [42] have compared RF and convolutional neural network (CNN) algorithms against the Water Cloud Model. The latter is driven by Sentinel-1 and -2 and the soil contribution was calculated only based on a simple empirical model instead of the Oh model as used in our investigation. Their finding revealed that CNN performed better than RF and WCM.

Overall, based on our findings, we can conclude that data-driven ML algorithms (SVR_rbf and ANN), particularly with only radar data can be a viable alternative to semiempirical parameterized models. As a matter of fact, in addition to a strong dependence of optical data to atmospheric perturbation, the driven of ML with radar data allow us to avoid the complexity between vegetation index and radar backscatter coefficient, especially in the case of small samples as stated in [43]. Additionally, as shown in our investigations, the performances of SVR_rbf and ANN algorithms were quite similar in all simulations. Nevertheless, SVR_rbf has great advantages compared to ANN. In point of fact, SVR_rbf exhibits low computation time and reduces the complexity of the modeling procedure during the training phase, as explained in [66]. Hence, in what follows, only SVR_rbf is chosen for SSM mapping.

C. SSM Mapping

The built SVR_rbf algorithm was implemented to map SSM over a large irrigated area called “R3 perimeter.” This area,

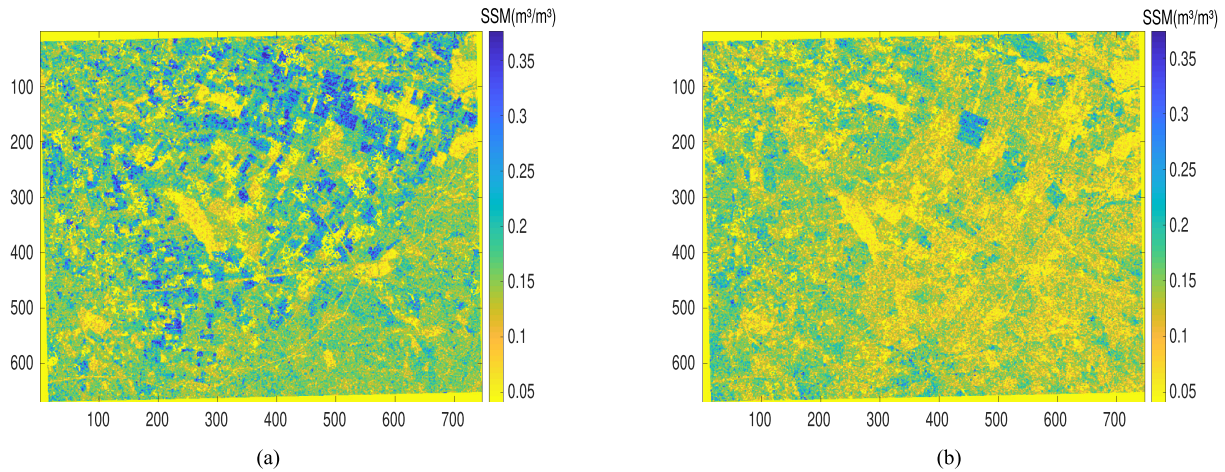


Fig. 8. SSM maps over an irrigated perimeter located 40 km east of Marrakech named R3 for two different SSM conditions. (a) Wet condition (Jan. 15, 2017). (b) Dry condition (Jun. 20, 2017).

which is situated within the Houaz plain, is located about 40 km east of Marrakech. It covers about 2800 ha and is mainly planted by wheat. Traditional flood irrigation is practiced by farmers using a network of concrete channels directly connected to a dam. Fig. 8 exhibits two maps of soil moisture obtained by running the SVR_rbf algorithm using Sentinel-1 images of backscatter coefficients and coherence at VV polarization, acquired at two dates with contrasting soil moisture during the 2016–2017 crop season. 1) Jan. 15, 2017, during the growing season when all wheat fields are irrigated. 2) Jun. 20, 2017, when all wheat fields have been harvested. By scrutinizing these two maps, one can clearly observe that most of the wheat fields were wet in January with SSM values reaching about $0.39 \text{ m}^3/\text{m}^3$. Likewise, this algorithm was able to highlight a high contrast in the variability of hydric conditions from one field to another due to irrigation distribution and sowing date. In fact, the irrigation of the total R3 sector takes approximately 12 days to generate, thus, a large heterogeneity in terms of the hydric condition along the sector. In contrast to January, drier conditions are observed in June where most of the fields are harvested. Overall, these maps elaborated only from radar data are in good accordance with the finding in [45] using WCM, which needs supplementary variables such as the surface roughness and fraction cover derived optical images. In addition to the difficulty related to the derivation of surface roughness at a large scale due to the heterogeneity of soil, our investigation showed that the SVR_rbf algorithm takes largely less time than WCM to generate one map over R3 (about a multiple of 20), which is an interesting advantage, particularly for generating maps at large scale and for long series of images.

IV. CONCLUSION

The aim of this work was to assess ML algorithms versus coupled WCM for SSM retrieval over wheat crops based on two complementary relatively independent information (i.e., backscatter coefficient and coherence) derived from Sentinel-1

data. The focus only on radar data has permitted us to get away from dependence on optical data that are restricted by weather and illumination conditions. A large in situ database gathered from several irrigated and rainfed wheat fields in Morocco and Tunisia is used in this work. Specifically, ML algorithms that were evaluated include single-layer ANN, DNN, three SVR models [viz., radial basis function (rbf), linear, and polynomial kernels], and two tree-based methods (viz. RF and XGBoost).

In the first step, all ML algorithms were trained and validated using data collected over several irrigated and rainfed wheat fields located in Morocco and Tunisia. Based on the comparison between estimated and measured SSM, it was found that ANN, DNN, SVR_rbf, and XGBoost were the best from each category algorithms to retrieve SSM with a good performance for VV polarization ($0.75 < R < 0.76$ and $\text{RMSE} = 0.05 \text{ cm}^3/\text{cm}^3$). In the second step, an investigation of the transferability of these algorithms is made using a second in situ dataset collected over a drip-irrigated wheat in Morocco. The investigation only focused on ANN, SVR_rbf, and XGBoost, as the highly complex DNN yielded comparable results. Overall, the ANN and rbf-based SVR algorithms showed to reasonably estimate SSM at VV polarization (R and RMSE of 0.81 and $0.034 \text{ m}^2/\text{m}^2$) and performed slightly better than XGBoost (R and RMSE of 0.76 and $0.038 \text{ m}^2/\text{m}^2$). Likewise, it was found that their performance is comparable to that revealed by the WCM model, which demonstrates their potential for retrieving SSM from only radar data. More precisely, due to its good compromise between retrieval accuracy of SSM, processing time, and simplicity, it can be concluded that SVR_rbf can be fairly used in the SSM inversion process instead of backscattering modeling even semiempirical ones, particularly for SSM mapping purposes. Indeed, our investigation revealed that generating an SSM map over a region with an area of $4 \times 4 \text{ km}^2$ using WCM took more time than the use of SVR_rbf (about a multiple of 20). Nonetheless, scientifically speaking, ML algorithms should in no way hinder the advancement of physical and semiempirical

backscatter models but rather support and complement their development. In fact, the use of these models is still inevitable, especially for radar signal comprehension over a complex vegetated canopy and the development of new generation of radars thanks to preliminary case studies before the launching phase.

As far as short-term prospects go, we intend to 1) apply ML algorithms to map root zone soil moisture by exploring the retrieved values of SSM obtained in this work, and, 2) assimilate these SSM values into LSMs in order to improve their continuous spatiotemporal soil moisture and evapotranspiration estimates.

APPENDIX ML ALGORITHMS

ANN and DNN

The ANNs establish a relationship between the input features and the expected output. This relationship is built by summing the weighted inputs and adjusting the weights until the desired output is obtained. In general, many ANN architectures are presented in the literature [67], each one consists of multiple neural layers, which are connected by their associated weights. Basically, these neurons comprise activation functions (usually nonlinear), which is used to establish ANN input–output relationship due to their ability to boost the learning power of an ANN model. The process of ANN algorithm consists first of getting the weighted combination output of a neuron (v_{ik}^l) using input signals (x_1, x_2, \dots, x_k) through a linear regression model as follows:

$$y_i^k = \sum_{j=1}^n w_{ij} x_j^{l-1} + b_i^l \quad (1)$$

where w_{ij} represents the interconnection weight between i th neuron in the current l th hidden-layer and the j th neuron of the previous ($l-1$)th hidden-layer, x_j^{l-1} represents the output of the previous layer or layer $l-1$ obtained using the current input of layer l , and finally, b_i^l is the bias term of the i th neuron of the l th hidden-layer. Second, an activation function is applied to the obtained output value of a hidden-layer's neuron in order to get output, which will be used afterward as an input for the next hidden layer. In practice, there are several activation functions, which allow us to introduce the property of nonlinearity into the model, such as sigmoid hyperbolic tangent and rectified linear unit (ReLU) functions. In this work, the ReLU activation function is used for the hidden layers due to its top performance computation compared to other activation functions as proved in [68]. This function is mathematically expressed as

$$g(y_i^k) = \max(0, y_i^k). \quad (2)$$

Finally, for the last hidden layer that connects to the output, a linear activation function is applied providing an output retrieved soil moisture (RSM) as follows:

$$\text{RSM} = g(y_{i=m}^{k=L}) = y_{i=m}^{k=L}. \quad (3)$$

In the training phase of the ANN model, the difference between RSM and MSM is minimized throughout adjusting the interconnection weights using a chosen objective function, which is a mean-squared error-based and is expressed as

$$L(\text{RSM}, \text{MSM}) = \sum_{n=1}^N (\text{RSM} - \text{MSM})^2 \quad (4)$$

where N is the number of soil moisture samples.

Deep learning (DNN) is a multilayer neural-network-based ML technique. In this work, we use CNN, which has a hierarchical architecture that consists of multiple layers of convolutional and pooling operations. They are able to learn local and global features in an image by applying filters to subsets of the input.

Support Vector Regression

SVR incorporates nonparametric kernel functions (Φ), which permit to obtain successful and effective results in modeling various relationships. Technically, these kernel functions are used in conjunction with an epsilon-insensitive loss function (ϵ -SVR) to perform a regression task. So, given a set of n input–output training data $[x_i, y_i], i = 1, 2, \dots, n, x \in R^k, y \in R$, the goal of the training algorithm is to construct a linear optimal function $f(x) = x'w + b$ (b is a bias and $w \in R^k$ are weights), that deviates from the obtained targets y_i by a value no greater than epsilon (ϵ) for all the training data and, at the same time, is as flat as possible. To do that, the norm value ($w'w$) should be minimized as a convex optimization problem, subject to the constraint that sets the absolute error in the predicted value of each of the training data less than or equal ϵ . This first minimization step uses a primal formula. Then, the constrained optimization problem is reformulated into a dual formula, which provides a lower bound to the solution given by the primal problem by introducing nonnegative Lagrange multipliers α_i and α_i^* for each observation x_i . In this work, three kernels functions are used and expressed as follows:

$$\Phi(x_i, x_j) = \begin{cases} \exp(-\gamma \|x_i - x_j\|^2) & \text{:RBF} \\ (1 + x_i'x_j)^d & \text{:Polynomial, } d \in \{2, 3, \dots\} \\ x_i'x_j & \text{:Linear} \end{cases} \quad (5)$$

Tree-Based Algorithms: RFR and XGboost Regression

RFR algorithm consists of creating each tree from a different sample of the training dataset. At each tree node, RFR selects a different sample of features for splitting and then runs the decision trees in parallel with no interaction among them. The predictions of all decision trees are averaged to increase the performance of the model. Given an input vector x , the RFR algorithm independently generates N regression trees $h_n(x), (n = 1, \dots, N)$, and the final model prediction (FMP) is given by the following equation:

$$\text{FMP} = \frac{1}{N} \sum_{n=1}^N h_n(x). \quad (6)$$

XGBoost is an ensemble technique that is also a tree-based algorithm and works through the use of the gradient boosting method.

The main difference between the two algorithms is that, as mentioned before, RFR builds several decision trees independently in parallel form at the training phase while XGboost creates decision trees in sequential form by selecting the first decision tree as its base learner. Then, by adding a new base learner trained using the residual's previous tree, the error between predictive values and target can be reduced. Finally, XGBoost uses an added model to combine the outputs of considered N decision trees in the algorithm to predict the final output as follows:

$$\text{FMP} = \sum_{n=1}^N h_n(x), h \in F \quad (7)$$

where h stands for a decision tree and F represents the function of all decision trees.

Semiempirical Models

Basically, the Water Cloud model, which aims to better simulate the backscattering coefficient of the vegetation canopies ($\sigma_{pq,\text{canopy}}^0$), is based on the radiation transport equation. In this model, the vegetation is considered to be homogeneous horizontal clouds, allowing multiple scattering to be ignored. Therefore, the total backscattering in canopy is presented only by the sum of two components: 1) scattering reflected directly from the vegetation, and, 2) scattering from the bare soil. Mathematically, the formulas of Water Cloud model are expressed as

$$\sigma_{pq,\text{canopy}}^0 = \sigma_{pq,\text{vegetation}}^0 + \tau^2 \sigma_{pq,\text{soil}}^0 \quad (8)$$

$$\sigma_{pq,\text{vegetation}}^0 = AV \cos \theta (1 - \tau^2) \quad (9)$$

$$\tau^2 = \exp(-2BV / \cos \theta) \quad (10)$$

where $\sigma_{pq,\text{vegetation}}^0$ and $\sigma_{pq,\text{soil}}^0$ denote the contribution of the vegetation and soil, respectively; pq is the polarization mode (V or H); τ^2 is the two-way transmissivity term of the vegetation layer; V is a parameter describing the vegetation canopy dynamics; θ is incident angle; A and B are empirical coefficients that strongly depend on canopy type, sensor frequency and polarization, and incidence angle. The values of A and B used in this study were 0.03448 and 1.034483, respectively. The Oh model is used to calculate soil contribution. Briefly, this model links the copolarized p ($= \sigma_{hh}^0 / \sigma_{vv}^0$) and cross-polarized q ($= \sigma_{vh}^0 / \sigma_{vv}^0$) ratios to radar wave incident angle (θ , in radians), wave number ($k = 2\pi/\lambda$ where λ is the wavelength), root-mean-square height (h_{rms}), and soil dielectric constant (ϵ_r). The latter was calculated from soil texture and soil moisture using an empirical model [69]. The following are the empirical expressions of σ_{vh}^0 , σ_{vv}^0 :

$$\sigma_{vv}^0 = g \cos^3 \theta \cdot [R_v + R_h] / \sqrt{p} \quad (11)$$

$$\sigma_{vh}^0 = q \sigma_{vv}^0 \quad (12)$$

where

$$q = 0.23(1 - \exp(-kh_{\text{rms}}))\sqrt{R_o} \quad (13)$$

$$\sqrt{p} = 1 - \exp(-kh_{\text{rms}}) \cdot (2\theta/\pi)^{[1/3R_o]} \quad (14)$$

$$g = 0.7 [1 - \exp(-0.65(kh_{\text{rms}})^{1.8})] \quad (15)$$

R_o , R_v , and R_h denote the Fresnel coefficients given by the following expressions: $R_o = \left| \frac{1 - \sqrt{\epsilon_r}}{1 + \sqrt{\epsilon_r}} \right|^2$, $R_v = \frac{\epsilon_r \cos \theta - \sqrt{\epsilon_r - \sin^2 \theta}}{(\epsilon_r \cos \theta - \sqrt{\epsilon_r - \sin^2 \theta})^2}$, and $R_h = \frac{\cos \theta - \sqrt{\epsilon_r - \sin^2 \theta}}{(\cos \theta - \sqrt{\epsilon_r - \sin^2 \theta})^2}$.

REFERENCES

- [1] R. Orth et al., "Global soil moisture data derived through machine learning trained with in-situ measurements," *Sci. Data*, vol. 8, pp. 1–14, 2021.
- [2] H. Vereecken, J. Huisman, H. Bogaen, J. Vanderborght, J. Vrugt, and J. Hopmans, "On the value of soil moisture measurements in vadose zone hydrology: A review," *Water Resour. Res.*, vol. 44, no. 4, pp. 1–21, 2008, doi: [10.1029/2008WR006829](https://doi.org/10.1029/2008WR006829).
- [3] Y. Chen and H. Yuan, "Evaluation of nine sub-daily soil moisture model products over China using high-resolution in situ observations," *J. Hydrol.*, vol. 588, 2020, Art. no. 125054.
- [4] Z. L. Li, P. Leng, C. Zhou, K. S. Chen, F. C. Zhou, and G. F. Shang, "Soil moisture retrieval from remote sensing measurements: Current knowledge and directions for the future," *Earth-Sci. Rev.*, vol. 218, 2021, Art. no. 103673.
- [5] P. R. Houser, W. J. Shuttleworth, J. S. Famiglietti, H. V. Gupta, K. H. Syed, and D. C. Goodrich, "Integration of soil moisture remote sensing and hydrologic modeling using data assimilation," *Water Resour. Res.*, vol. 34, pp. 3405–3420, 1998.
- [6] O. Merlin, A. Chehbouni, G. Boulet, and Y. Kerr, "Assimilation of disaggregated microwave soil moisture into a hydrologic model using coarse-scale meteorological data," *J. Hydrometeorol.*, vol. 7, pp. 1308–1322, 2006.
- [7] C. Massari, L. Brocca, T. Moramarco, Y. Tramblay, and J. F. D. Lescot, "Potential of soil moisture observations in flood modelling: Estimating initial conditions and correcting rainfall," *Adv. Water Resour.*, vol. 74, pp. 44–53, 2014.
- [8] H. Lievens et al., "SMOS soil moisture assimilation for improved hydrologic simulation in the Murray Darling Basin, Australia," *Remote Sens. Environ.*, vol. 168, pp. 146–162, 2015.
- [9] L. Liu, T. Ao, and L. Zhou, "Improving the initial conditions of hydrological model with reanalysis soil moisture data," *EGU Sphere*, vol. 452, pp. 1–38, 2022.
- [10] P. Mason et al., "Implementation plan for the global observing system for climate in support of the UNFCCC (2010 update, DRAFT v1.0, 13 November 2009)," pp. 1–153, 2010. [Online]. Available: <http://www.ecopuerto.com/bicentenario/informes/PlanClima-Cop15.pdf>
- [11] J. Martínez-Fernández, A. González-Zamora, N. Sánchez, A. Gumuzzio, and C. Herrero-Jiménez, "Satellite soil moisture for agricultural drought monitoring: Assessment of the SMOS derived soil water deficit index," *Remote Sens. Environ.*, vol. 177, pp. 277–286, 2016.
- [12] C. Champagne, J. White, A. Berg, S. Belair, and M. Carrera, "Impact of soil moisture data characteristics on the sensitivity to crop yields under drought and excess moisture conditions," *Remote Sens.*, vol. 11, 2019, Art. no. 372.
- [13] V. Naeimi, K. Scipal, Z. Bartalis, S. Hasenauer, and W. Wagner, "An improved soil moisture retrieval algorithm for ERS and METOP scatterometer observations," *IEEE Trans. Geosci. Remote Sens.*, vol. 47, no. 7, pp. 1999–2013, Jul. 2009.
- [14] E. Njoku, *AMSR-E/Aqua Daily L3 Surface Soil Moisture, Interpretive Parameters, QC EASE-Grids, Version 2*. Boulder, CO, USA: NASA Nat. Snow Ice Data Center Distributed Active Arch. Center, 2004, doi: [10.5067/AMSR-E/AE_LAND3.002](https://doi.org/10.5067/AMSR-E/AE_LAND3.002).
- [15] Y. H. Kerr, P. Waldteufel, J. P. Wigneron, J. Martinuzzi, J. Font, and M. Berger, "Soil moisture retrieval from space: The soil moisture and ocean salinity (SMOS) mission," *IEEE Trans. Geosci. Remote Sens.*, vol. 39, no. 8, pp. 1729–1735, Aug. 2001.
- [16] J. Chaubell et al., "Regularized dual-channel algorithm for the retrieval of soil moisture and vegetation optical depth from SMAP measurements," *IEEE J. Sel. Topics Appl. Earth Observ. Remote Sens.*, vol. 15, pp. 102–114, Oct. 2022, doi: [10.1109/JSTARS.2021.3123932](https://doi.org/10.1109/JSTARS.2021.3123932).
- [17] L. Pasolli et al., "Soil moisture monitoring in mountain areas by using high-resolution SAR images: Results from a feasibility study," *Eur. J. Soil Sci.*, vol. 65, pp. 852–864, 2014.
- [18] A. Moreira, P. Prats-Iraola, M. Younis, G. Krieger, I. Hajnsek, and K. P. Papathanassiou, "A tutorial on synthetic aperture radar," *IEEE Geosci. Remote Sens. Mag.*, vol. 1, no. 1, pp. 6–43, Mar. 2013.
- [19] E. Santi, S. Paloscia, S. Pettinato, and G. Fontanelli, "Application of artificial neural networks for the soil moisture retrieval from active and passive microwave spaceborne sensors," *Int. J. Appl. Earth Observ. Geoinformation*, vol. 48, pp. 61–73, 2016.

- [20] R. Torres et al., "GMES Sentinel-1 mission," *Remote Sens. Environ.*, vol. 120, pp. 9–24, 2012.
- [21] R. Meyer et al., "Exploring the combined use of SMAP and Sentinel-1 data for downscaling soil moisture beyond the 1 km scale," *Hydrol. Earth Syst. Sci.*, vol. 26, pp. 3337–3357, 2022.
- [22] F. T. Ulaby, K. Sarabandi, K. McDonald, M. Whitt, and M. C. Dobson, "Michigan microwave canopy scattering model," *Int. J. Remote Sens.*, vol. 11, pp. 1223–1253, 1990.
- [23] M. A. Karam, A. K. Fung, R. H. Lang, and N. S. Chauhan, "A microwave scattering model for layered vegetation," *Universities Space Res. Assoc., Goddard Visiting Scientist Program Space Earth Sci. Directorate, Tech. Rep. 93N18074*, 1992.
- [24] X. Song, J. Ma, X. Li, P. Leng, F. Zhou, and S. Li, "First results of estimating surface soil moisture in the vegetated areas using ASAR and Hyperion data: The Chinese Heihe River Basin case study," *Remote Sens.*, vol. 6, pp. 12055–12069, 2014.
- [25] Y. Oh, K. Sarabandi, and F. T. Ulaby, "An empirical model and an inversion technique for radar scattering from bare soil surfaces," *IEEE Trans. Geosci. Remote Sens.*, vol. 30, pp. 370–381, Mar. 1992, doi: [10.1109/36.134086](https://doi.org/10.1109/36.134086).
- [26] E. Attema and F. T. Ulaby, "Vegetation modeled as a water cloud," *Radio Sci.*, vol. 13, pp. 357–364, 1978.
- [27] R. Bindlish and A. P. Barros, "Parameterization of vegetation backscatter in radar-based, soil moisture estimation," *Remote Sens. Environ.*, vol. 76, pp. 130–137, 2001.
- [28] I. Gherboudj, R. Magagi, A. A. Berg, and B. Toth, "Soil moisture retrieval over agricultural fields from multi-polarized and multi-angular RADARSAT-2 SAR data," *Remote Sens. Environ.*, vol. 115, pp. 33–43, 2011.
- [29] M. El Hajj et al., "Soil moisture retrieval over irrigated grassland using X-band SAR data," *Remote Sens. Environ.*, vol. 176, pp. 202–218, 2016.
- [30] M. Hosseini and H. McNairn, "Using multi-polarization C-and L-band synthetic aperture radar to estimate biomass and soil moisture of wheat fields," *Int. J. Appl. Earth Observ. Geoinformation*, vol. 58, pp. 50–64, 2017.
- [31] S. Bousbih et al., "Potential of Sentinel-1 radar data for the assessment of soil and cereal cover parameters," *Sensors*, vol. 17, 2017, Art. no. 2617.
- [32] H. Wang, R. Magagi, and K. Goita, "Potential of a two-component polarimetric decomposition at C-band for soil moisture retrieval over agricultural fields," *Remote Sens. Environ.*, vol. 217, pp. 38–51, 2018.
- [33] R. Attarzadeh, J. Amini, C. Notarnicola, and F. Greifeneder, "Synergetic use of Sentinel-1 and Sentinel-2 data for soil moisture mapping at plot scale," *Remote Sens.*, vol. 10, no. 8, 2018, Art. no. 1285.
- [34] C. Ma, X. Li, and M. F. McCabe, "Retrieval of high-resolution soil moisture through combination of Sentinel-1 and Sentinel-2 data," *Remote Sens.*, vol. 12, no. 14, 2020, Art. no. 2303.
- [35] H. Srivastava, P. Patel, R. Navalgund, and Y. Sharma, "Retrieval of surface roughness using multi-polarized Envisat-1 ASAR data," *Geocarto Int.*, vol. 23, pp. 67–77, 2008.
- [36] L. Dong, W. Wang, R. Jin, F. Xu, and Y. Zhang, "Surface soil moisture retrieval on Qinghai-Tibetan plateau using Sentinel-1 synthetic aperture radar data and machine learning algorithms," *Remote Sens.*, vol. 15, 2023, Art. no. 153.
- [37] L. Karthikeyan, M. Pan, N. Wanders, D. N. Kumar, and E. F. Wood, "Four decades of microwave satellite soil moisture observations: Part 1. A review of retrieval algorithms," *Adv. Water Resour.*, vol. 109, pp. 106–120, 2017.
- [38] I. Ali, F. Greifeneder, J. Stamenkovic, M. Neumann, and C. Notarnicola, "Review of machine learning approaches for biomass and soil moisture retrievals from remote sensing data," *Remote Sens.*, vol. 7, pp. 16398–16421, 2015.
- [39] Q. Yuan, H. Xu, T. Li, H. Shen, and L. Zhang, "Estimating surface soil moisture from satellite observations using a generalized regression neural network trained on sparse ground-based measurements in the continental US," *J. Hydrol.*, vol. 580, 2020, Art. no. 124351.
- [40] M. El Hajj, N. Baghdadi, M. Zribi, and H. Bazzi, "Synergic use of Sentinel-1 and Sentinel-2 images for operational soil moisture mapping at high spatial resolution over agricultural areas," *Remote Sens.*, vol. 9, 2017, Art. no. 1292.
- [41] A. K. Holtgrave, M. Förster, F. Greifeneder, C. Notarnicola, and B. Klein-schmit, "Estimation of soil moisture in vegetation-covered floodplains with Sentinel-1 SAR data using support vector regression," *PFG—J. Photogrammetry, Remote Sens., Geoinformation Sci.*, vol. 86, pp. 85–101, 2018.
- [42] R. Inoubli, L. Bennaceur, N. Jarray, A. Ben Abbes, and I. Farah, "A comparison between the use of machine learning techniques and the water cloud model for the retrieval of soil moisture from Sentinel-1A and Sentinel-2A products," *Remote Sens. Lett.*, vol. 13, pp. 980–990, 2022.
- [43] J. Zhao, C. Zhang, L. Min, Z. Guo, and N. Li, "Retrieval of farmland surface soil moisture based on feature optimization and machine learning," *Remote Sens.*, vol. 14, 2022, Art. no. 5102.
- [44] N. Efreimova, M. E. A. Seddik, and E. Erten, "Soil moisture estimation using Sentinel-1/2 imagery coupled with cycleGAN for time-series gap filing," *IEEE Trans. Geosci. Remote Sens.*, vol. 60, pp. 1–11, Dec. 2021, doi: [10.1109/TGRS.2021.3134127](https://doi.org/10.1109/TGRS.2021.3134127).
- [45] N. Ouadi et al., "Monitoring of wheat crops using the backscattering coefficient and the interferometric coherence derived from Sentinel-1 in semi-arid areas," *Remote Sens. Environ.*, vol. 251, 2020, Art. no. 112050.
- [46] A. Villarroya-Carpio, J. M. Lopez-Sanchez, and M. E. Engdahl, "Sentinel-1 interferometric coherence as a vegetation index for agriculture," *Remote Sens. Environ.*, vol. 280, 2022, Art. no. 113208.
- [47] U. Wegmuller and C. Werner, "Retrieval of vegetation parameters with SAR interferometry," *IEEE Trans. Geosci. Remote Sens.*, vol. 35, no. 1, pp. 18–24, Jan. 1997.
- [48] M. E. Engdahl, M. Borgeaud, and M. Rast, "The use of ERS-1/2 tandem interferometric coherence in the estimation of agricultural crop heights," *IEEE Trans. Geosci. Remote Sens.*, vol. 39, no. 8, pp. 1799–1806, Aug. 2001.
- [49] X. Blaes and P. Defourny, "Retrieving crop parameters based on tandem ERS 1/2 interferometric coherence images," *Remote Sens. Environ.*, vol. 88, pp. 374–385, 2003.
- [50] J. Ezzahar et al., "Evaluation of backscattering models and support vector machine for the retrieval of bare soil moisture from Sentinel-1 data," *Remote Sens.*, vol. 12, 2019, Art. no. 72.
- [51] N. Ouadi et al., "C-band radar data and in situ measurements for the monitoring of wheat crops in a semi-arid area (center of Morocco)," *Earth Syst. Sci. Data*, vol. 13, pp. 3707–3731, 2021.
- [52] CNES, *The ORFEO Tool Box Software Guide*, 2018.
- [53] M. Nuno and P. J. Meadows, "Radiometric calibration of S-1 level-1 products generated by the S-1 IPF," 2015. [Online]. Available: <https://sentinel.esa.int/documents/247904/685163/S1-Radiometric-Calibration-V1.0.pdf>
- [54] D. Small, "Flattening gamma: Radiometric terrain correction for SAR imagery," *IEEE Trans. Geosci. Remote Sens.*, vol. 49, no. 8, pp. 3081–3093, Aug. 2011.
- [55] D. Small and A. Schubert, "Guide to ASAR geocoding," *ESA-ESRIN, Frascati, Italy, Tech. Rep. RSL-ASAR-GC-AD*, vol. 1, pp. 1–36, 2008. [Online]. Available: <https://dokumen.tips/download/link/guide-to-asar-geocoding-university-of-zurich-guide-to-asar-geocoding-issue-101.html>
- [56] P. Patel, H. S. Srivastava, S. Panigrahy, and J. S. Parihar, "Comparative evaluation of the sensitivity of multi-polarized multi-frequency SAR backscatter to plant density," *Int. J. Remote Sens.*, vol. 27, pp. 293–305, 2006.
- [57] S. Chauhan and H. S. Srivastava, "Comparative evaluation of the sensitivity of multi-polarized SAR and optical data for various land cover classes," *Int. J. Adv. Remote Sens., GIS, Geogr.*, vol. 4, pp. 1–14, 2016.
- [58] Y. Bao, L. Lin, S. Wu, K. A. K. Deng, and G. P. Petropoulos, "Surface soil moisture retrievals over partially vegetated areas from the synergy of Sentinel-1 and Landsat 8 data using a modified water-cloud model," *Int. J. Appl. Earth Observ. Geoinformation*, vol. 72, pp. 76–85, 2018.
- [59] T. L. Passafaro et al., "Would large dataset sample size unveil the potential of deep neural networks for improved genome-enabled prediction of complex traits? The case for body weight in broilers," *BMC Genomic.*, vol. 21, pp. 1–13, 2020.
- [60] K. O. Achieng, "Modelling of soil moisture retention curve using machine learning techniques: Artificial and deep neural networks vs support vector regression models," *Comput. Geosci.*, vol. 133, 2019, Art. no. 104320.
- [61] J. Jin et al., "Support vector regression for high-resolution beach surface moisture estimation from terrestrial Lidar intensity data," *Int. J. Appl. Earth Observ. Geoinformation*, vol. 102, 2021, Art. no. 102458.
- [62] T. Katagis, D. Fernández-Prieto, M. Marconcini, and W. Dorigo, "In soil moisture estimation by using active microwave measurements and support vector regression (SVR)," in *Proc. Earsel Symp.*, 2013, pp. 1–8. [Online]. Available: http://www.earsel.org/symposia/2013-symposium-Matera/pdf_proceedings/EARSeL-Symposium-2013_4_8_thomaskatagis.pdf
- [63] T. T. Nguyen et al., "A low-cost approach for soil moisture prediction using multi-sensor data and machine learning algorithm," *Sci. Total Environ.*, vol. 833, 2022, Art. no. 155066.
- [64] K. E. Taylor, "Summarizing multiple aspects of model performance in a single diagram," *J. Geophys. Res.*, vol. 106, pp. 7183–7192, 2001.
- [65] M. Zribi, N. Baghdadi, N. Holah, O. Fafin, and C. Guérin, "Evaluation of a rough soil surface description with ASAR-ENVISAT radar data," *Remote Sens. Environ.*, vol. 95, no. 1, pp. 67–76, 2005.

- [66] M. K. Gill, T. Asefa, M. W. Kemblowski, and M. McKee, "Soil moisture prediction using support vector machines," *J. Amer. Water Resour. Assoc.*, vol. 42, pp. 1033–1046, 2006.
- [67] I. Goodfellow, Y. Bengio, and A. Courville, *Deep Learning*. Cambridge, MA, USA: MIT Press, 2016.
- [68] Q. Su et al., "A probabilistic framework for nonlinearities in stochastic neural networks," in *Proc. Adv. Neural Inf. Process. Syst.*, vol. 30, pp. 1–10, 2017. [Online]. Available: https://proceedings.neurips.cc/paper_files/paper/2017/file/35936504a37d53e03abdfbc7318d9ec7-Paper.pdf
- [69] M. T. Hallikainen, F. T. Ulaby, M. C. Dobson, M. A. El-Rayes, and L. K. Wu, "Microwave dielectric behavior of wet soil—Part 1: Empirical models and experimental observations," *IEEE Trans. Geosci. Remote Sens.*, vol. GE-23, no. 1, pp. 25–34, Jan. 1985.



Jamal Ezzahar received the Ph.D. degree in physics from the Faculty of Sciences Semlalia, Cadi Ayyad University, Marrakesh, Morocco, in 2007.

He is currently a permanent Professor with the Department of Computer Science, Networks and Telecommunications, National School of Applied Sciences Safi, Safi, Morocco. His research interests include soil moisture, turbulent fluxes, machine learning, multisource remote sensing imagery, and coupled land–atmosphere systems modeling for land applications in semiarid regions.



Abdelghani Chehbouni received the B.S. degree in fluids mechanics from University Paul Sabatier, Toulouse, France, in 1987, the M.S. degree in environment science from the National Polytechnic Institute of Toulouse, Toulouse, in 1989, and the Ph.D. degree in hydrology and remote sensing from University Paul Sabatier in 1992.

He has been working with the University of Arizona, Tucson, AZ, USA, for 18 months and the Jet Propulsion Laboratory for 2 years. He is a coinventor of several remote sensing programs (VEGETATION, ERS2/ATSR2, and EOS). He has participated in several international experiments (MONSOON'90, Hapex Sahel) and was a coleader of the Semi-Arid-Land-Surface-Atmosphere international program. He joined CESBIO in 2000 as the leader of hydrology group. He is currently the Director of the Center for Remote Sensing Applications and the International Water Research Institute, Mohammed VI Polytechnic University. His main research interests include the application of remotely sensed data in land–surface–atmosphere models, especially in arid semiarid regions.



Nadia Ouadi received the B.S. degree in mathematics, computer science, and physics from the Faculty of Sciences and Techniques, Sultan Moulay Slimane University, Beni Mellal, Morocco, in 2015, the M.S. degree in mechanics of fluids and energetics from the Faculty of Sciences Semlalia, Cadi Ayyad University, Marrakesh, Morocco, in 2017, and the Ph.D. degree in remote sensing and water resources management jointly from Paul Sabatier University, Toulouse, France, and Cadi Ayyad University in 2021.

She is currently a Postdoctoral Researcher with the French National Center for Scientific Research (CNRS) and has been with the Center for the Study of the Biosphere from Space (CESBIO) since November 2021. She is working on the processing and exploitation of SAR polarimetry and interferometry data for monitoring the hydric conditions of annual crops.



Mohammed Madiafi received the M.S. degree in information processing and the Ph.D. degree in artificial intelligence from Hassan II Mohammedia-Casablanca University, Casablanca, Morocco, in 2008 and 2013, respectively.

He is currently an Assistant Professor with Cadi Ayyad University, Marrakech, Morocco. His current research interests include deep learning, artificial neural networks, fuzzy and intelligent systems, evolutionary algorithms, pattern classification and recognition, unsupervised learning, and data compression.



Khabba Said received the Ph.D. degree in water sciences from Cadi Ayyad University, Marrakech, Morocco, in 2001.

He has been a Senior Lecturer with the Faculty of Sciences Semlalia, Cadi Ayyad University, since 1996. He is currently an Eco-physiologist and has a background in agro-climatology and modeling. He has key expertise in micrometeorology and crops water requirement. The approach used is based on the synergy between field measurements, simple and complex modeling, and satellite observations (multi-sensor and multiresolution). He has authored or coauthored more than 80 papers in international peer-reviewed journals and has supervised 7 Ph.D. students. His research interest includes modeling crop growth, development, and yield in semiarid areas.



Salah Er-Raki (Member, IEEE) received the Ph.D. degree in physics from the Faculty of Sciences Semlalia, Cadi Ayyad University, Marrakesh, Morocco, in 2007.

He is currently a Professor of Physics with the Faculty of Sciences and Techniques, Cadi Ayyad University, Marrakesh, Morocco. He has supervised and cosupervised eight Ph.D. students. His research interests include physique, irrigation, agricultural sciences, remote sensing, and geoscience.

Dr. Er-Raki is an editorial board member and a reviewer of many international scientific journals with high impact factor among them are *Agricultural Water Management*, *Remote Sensing of Environment*, *Remote Sensing*, and *Agricultural and Forest Meteorology*.



Ahmed Laamrani received the Ph.D. degree in environmental sciences from the University of Quebec in Montreal (UQAM), Montreal, QC, Canada, in 2014, and the University of Abitibi-Témiscamingue (UQAT), Rouyn-Noranda, QC, Canada.

He joined CRSA/UM6P in 2019 as a Professor specializing in soil remote sensing (RS) and applied geographic information systems (GIS). Prior to joining UM6P, he was a Researcher in RS and GIS from 2014 to 2017 with Agriculture and Agri-Food Canada and the University of Guelph from 2017 to 2019 in Canada, on agricultural soil RS and GIS projects. He has authored or coauthored several papers in refereed journals and attended/participated many international conferences. He has supervised and/or cosupervised many undergraduate and graduate students and trained several technicians. He is currently an Adjunct Professor in forest soil RS and GIS with UQAT. He has a solid foundation in the uses of RS and GIS for natural resources management, which includes advanced academic and research training. His research interests during the last five years sit at a crossroads between RS, GIS, drones, and agricultural soil cover with a focus on developing solutions for agricultural best management practices.



Adnane Chakir received the master's degree in engineering of solar thermal systems from Cadi Ayyad University, Marrakesh, Morocco, in 2019, where he is currently working toward the Ph.D. degree in the use of radar for detecting water stress over olive and wheat canopies in Morocco.

He works on the use of radar for detecting water stress over olive and wheat canopies in Morocco.



Zohra Lili Chabaane received the double master's degree in rural engineering from Tunisian National Agronomic Institute (INAT), Tunis, Tunisia, and the Engineering degree in hydraulic and agricultural climatology and the Ph.D. degree in physics – remote sensing, rural, and process engineering, from ENSA-Rennes, Rennes, France, in 1989 and 1993, respectively.

She is currently a Professor in rural engineering water and forest with the University of Carthage (UCAR)/ INAT. In 1997, she joined the Tunisian

National Agronomic Institute, University of Carthage, Carthage, Tunisia, where she is the in charge of courses of "remote sensing, GIS, spatial analysis, and water resources management." She is an expert and specialized in remote sensing, GIS, and spatial analysis for agricultural and water resources management. She was involved in more than 33 international projects (H2020, PRIMA, ERANETMED, UE FP6, UE FP7, ANR, AUF, ACDI, PHC Maghreb, TEMPUS, and ERASMUS+) and coordinated some of them. Her research interests include remote sensing and GIS applied to agricultural water resources management and agriculture in a context of climate changes.



Mehrez Zribi (Senior Member, IEEE) received the B.E. degree in signal processing from the Ecole Nationale Supérieure d'Ingénieurs en Constructions Aéronautiques, Toulouse, France, in 1995, and the Ph.D. degree in remote sensing and signal processing from the Université Paul Sabatier, Toulouse, in 1998.

He is currently a Research Director with Centre National de Recherche Scientifique, Paris, France. In 1995, he joined the Centre d'Etude des Environnements Terrestre et Planétaires Laboratory/Institut Pierre Simon Laplace, Vélizy, France. Since October

2008, he has been with the Centre d'Etudes Spatiales de la Biosphère (CESBIO), Toulouse. He is currently a Director of CESBIO. He has authored or coauthored more than 150 articles in refereed journals. His research interests include microwave remote sensing applied to hydrology, microwave modeling for land surface parameter estimations, and airborne microwave instrumentation.